PAPER

Check for updates

Stable lead-halide perovskite quantum dots as efficient visible light photocatalysts for organic transformations†

Sajan Pradhan,[a] Deshaj Bhujel,[a] Bikram Gurung,[a] Debesh Sharma,[a] Siddhant Basel,[a] Sagarmani Rasaily,[a] Surakcha Thapa,[a] Sukanya Borthakur,[b] Wai Li Ling, [c] Lakshi Saikia, [b] Peter Reiss, [c] Anand Pariyar [a] and Sudarsan Tamang [*a]

Lead halide perovskite (LHP) based colloidal quantum dots (**CQDs**) have tremendous potential for photocatalysis due to their exceptional optical properties. However, their applicability in catalysis is restricted due to poor chemical stability and low recyclability. We report halide-passivated, monodisperse $CsPbBr_3$ **CQDs** as a stable and efficient visible-light photocatalyst for organic transformations. We demonstrate oxidative aromatization of a wide range of heterocyclic substrates including examples which are poor hydrogen transfer (HAT) reagents. Two to five-fold higher rate kinetics were observed for reactions catalyzed by $CsPbBr_3$ **CQDs** in comparison with bulk-type $CsPbBr_3$ (**PNCs**) or conventionally synthesized $CsPbBr_3$ **CQDs** and other metal organic dyes (rhodamine 6G and $[Ru(bpy)_3]^{2+}$). Furthermore, these **CQDs** exhibit improved air-tolerance and photostability and in turn show a higher turnover number (TON) of 200, compared to conventionally prepared **CQDs** (TON = 166) and state-of-the-art bulk-type perovskite-based catalyst (TON = 177). Our study paves the way for the practical applicability of energy-level tunable, size-controlled LHP **CQDs** as efficient photocatalysts in organic synthesis.

Introduction

Lead halide perovskites (LHPs) have exceptional light absorbing/emitting properties.[1–5] In particular, the ability of LHPs to facilitate efficient charge separation and transfer upon photon absorption[6] has been extensively explored in the domain of photovoltaics[7–11] with power conversion efficiencies approaching the theoretical limit.[12,13] These unique photophysical properties of LHPs are also very appealing for activating organic substrates in photoredox catalysis where light absorption, charge separation and transfer are equally important.[14–19] LHP based colloidal quantum dots (**CQDs**) with well-defined size and shape, prepared for example by the hot-injection method,[20] may have additional advantages compared to larger sized and polydisperse LHP nanocrystals (**PNCs**) in photocatalysis: first, naturally they have a larger surface area and the energy levels can be tuned as a function of size[9,21,22] to control electronic transfer processes with the substrates. Second, these **CQDs** are highly dispersible in many organic solvents forming a homogeneous colloidal solution, yet with heterogeneous catalytic attributes such as recyclability and separability. And third, due to their monodisperse, well-defined size, shape and surface morphology, surface facet-controlled catalysis[23–25] with high specificity and affinity for various substrates could be explored. Unfortunately, conventionally prepared size- and shape-controlled LHP **CQDs** have poor air and moisture stability,[14,18] limiting their practical application in the photocatalysis. Furthermore, these nanocrystals are typically prepared in small scale compared to their bulk or polydisperse counterparts.[14,18] In fact, so far efficient photocatalysis of organic transformations were all achieved using highly polydisperse LHP **PNCs** (*ca.* 2–100 nm) with an average size too large to be in quantum confinement regime.[14,18] Conventionally prepared colloidal LHP **CQDs,** in turn, exhibited poor catalytic efficiency due to their poor tolerance of moisture, oxygen, substrates and solvents compared to these larger sized **PNCs.** In the literature, various strategies to improve air and moisture stability of LHPs can be found, specially of $CsPbI_3$ and $CsPbBr_3$ based perovskites. These strategies encompass the use of additives such as halide salt,[26] phosphinic acid,[27] ammonium halide,[28] 2,2′-iminodibenzoic acid,[29] sulphides and metal ions[30] and polymers[31] or imply the application of specific post-synthetic purification steps.[9,32] While these approaches have

[a]*Department of Chemistry, School of Physical Sciences, Sikkim University, Sikkim 737102, India*

[b]*Department of Material Science, North East Institute of Science and Technology (NEIST), Assam 785006, India*

[c]*Univ. Grenoble Alpes, CEA, CNRS, IRIG/SyMMES/STEP, 38000 Grenoble, France*

led to improved performances of LHP based optoelectronic devices (*e.g.*, solar cells, LEDs), they could not yet be exploited in the field of photocatalysis.

Herein, we report the use of halide passivated air-stable, CsPbBr₃ perovskite **CQDs** for the synthesis of a broad range of azaheterocycles *via* oxidative aromatization. Photocatalytic aromatization reactions involving nitrogen heterocycles such as 1,2-dihydropyridines (1,2-DHP), 1,4-dihydropyridines (1,4-DHP), dihydrobenzothiazoles and pyrazolines are important, however, kinetically slow reactions, requiring a strong oxidant and/or efficient catalyst. Although, air is a benign source of molecular oxygen which can act as an oxidant in the singlet state,[33–35] conventionally prepared perovskite-based **CQDs** and bulk halide perovskites are highly sensitive to O₂ and moisture, limiting their use in photocatalysis.[14,18,36,37] We demonstrate the practical applicability of monodispersed, air-stable CsPbBr₃ **CQDs** prepared using the individual Cs, Pb and Br precursors ("three precursors method") in the oxidative aromatization of azaheterocycles under visible light in open air. The nitrogen containing heterocycles (substrates) and heteroaromatics (products) under study in this report form a highly important class of organic compounds with ubiquitous presence in bioactive natural products or pharmaceutical drugs[38–42] and are at the same time the prototypes for the study of biochemical redox reactions.[43–45] Previous studies, which mostly focused on the aromatization of 1,2-dihydropyridine (1,2-DHP), 1,4-DHP and 1,3,5-triaryl-pyrazolines as substrates, used Ru-, Pd-, and Pt-based molecular catalysts with some degree of success,[45–48] however, at the cost of the use of expensive metal complexes

exhibiting oxygen intolerance, absence of recyclability, and fixed redox potentials.

Results and discussion

Synthesis and characterization of air-stable photocatalyst

Air-stable, halide-passivated CsPbBr₃ NCs (**QD1**) were prepared under optimized and scaled-up conditions *via* the "three precursors method" using bromine/oleylamine solution as bromide source based on our previous report (*cf.* ESI†).[22] As opposed to the conventional "two precursors method"[20] where three elements (*viz.*, Cs, Pb and Br) are obtained from two precursors (*viz.*, Cs-oleate and PbBr₂), the "three precursors method" allows for independent tuning of all three elements and achieving the desired halide-rich synthetic conditions.[22,49,50] **QD1** was prepared under halide-excess condition (Cs : Pb : Br ∼ 1 : 1 : 6) at high temperature (200 °C), based on the detailed reaction conditions-stability correlation study from our previous report.[22] The colloidal dispersion of **QD1** in hexane exhibited a UV-Vis absorption peak at 505 nm and a PL emission peak at 517 nm with an optical band gap of 2.46 eV (Fig. 1a). **QD1** exhibits long-term stability in ambient air conserving fluorescence quantum yield (Fig. S1 and S2†). TEM studies show that the nanocrystals have an edge length ∼9.4 ± 0.4 nm (Fig. 1b), which is in the moderate to weak quantum confinement regime.[51] Increasing the size of NCs to ∼15.7 ± 0.7 nm (**QD2**, Fig. S3a and b†) led to a slight red-shift of the emission maximum (521 nm) and decreasing the size to ∼7.2 ± 0.5 nm (**QD3**, Fig. S3c and d†) resulted in a blue shift (510 nm) attributed to the quantum confinement effect.[51–54] In
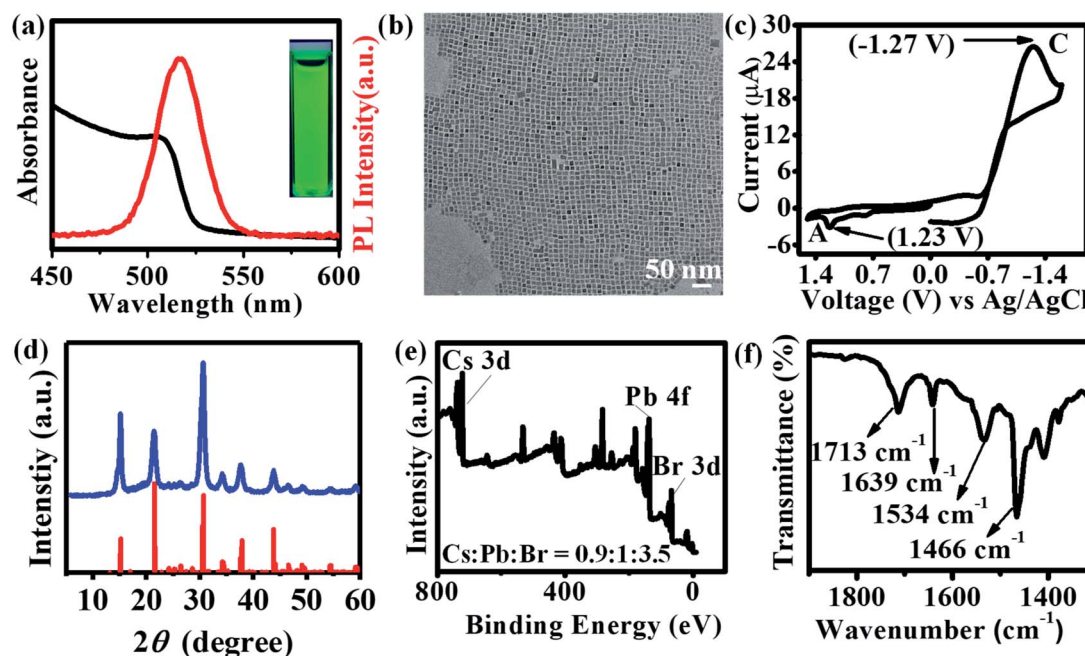

Fig. 1 Characterization of the CsPbBr₃ perovskite QDs (**QD1**): (a) UV-Vis absorption (black) and photoluminescence emission (red) spectra of the colloidal dispersion (excitation wavelength: 400 nm), inset: colloidal solution under UV lamp; (b) TEM image (cube edge length = ∼9.4 ± 0.4 nm); (c) cyclic voltammogram of the nanocrystals dispersed in acetonitrile/toluene (1 : 4) solution using tetrabutylammonium perchlorate (TBAP) as supporting electrolyte with a scan rate of 50 mV s⁻¹; (d) powder X-ray diffractogram of the QDs indexed to orthorhombic phase (JCPDS no. 00-054-0752) indicated as red bar; (e) XPS survey spectrum; (f) FTIR spectrum.

photocatalysis, the knowledge of the relative energy level positions of the catalyst with respect to the substrate is crucial for evaluating and maximizing the driving force of the reaction.[18] Cyclic voltammetry (CV) was used to determine the valence band maximum (VBM) and conduction band minimum (CBM) of the QDs.[55] The cyclic voltammogram of **QD1** (Fig. 1c) shows the anodic peak (A) at 1.23 V and cathodic peak (C) at −1.27 V for one complete cycle. The peak potential difference between these two peaks (A–C) results in an electrochemical bandgap of 2.50 eV, which is consistent with the obtained optical bandgap of **QD1**.[55] The exceptional air-stability of these **CQDs** (Fig. 1d) is attributed to halide/amine passivated surfaces as confirmed by X-ray photoelectron spectroscopy (XPS) and Fourier transform infrared spectroscopy (FTIR)[22] (Fig. 1e and f). The Pb 4f core level spectra of **QD1** show peaks at 138.39 and 143.25 eV assigned to the Pb $4f_{7/2}$ and Pb $4f_{5/2}$ levels, respectively. These values are slightly higher than for conventional $CsPbBr_3$ NCs (**QD4**) which show peaks at 138.34 and 143.20 eV (Fig. S4c†). This increase in binding energy value (shift by 0.05 eV) is consistent with literature reports for halide-ion rich $CsPbBr_3$ NCs.[22,26] The analysis of the Cs 3d, Pb 4f, and Br 3d peaks further confirmed that **QD1** displays a higher bromide ion rich surface (Cs : Pb : Br ∼ 0.9 : 1 : 3.5, Fig. 1e) in comparison to the **QD4** (Cs : Pb : Br ∼ 1.2 : 1 : 2.7, Fig. S4b†). Bromine is a volatile liquid and to ensure sufficient bromine precursor, we used excess of bromine (∼6 times) compared to Pb or Cs precursor. Fig. 1f shows a characteristic FTIR band at 1639 cm^{-1} confirming the presence of protonated amine groups (–NH$_3^+$). This observation, taken together with XPS results, confirm the presence of oleylammonium halide on the NC surface which is crucial for stability.[56] In addition, the peaks at 1713 cm^{-1} and 1534 cm^{-1} are attributed to the C=O stretching (free acid) and oleate anion (surface-bound) vibrations respectively.[57] The strong peak at 1466 cm^{-1} is due to bending vibration of C–H in CH_2 group which is integral part of the ligands. Importantly, **QD1** showed improved photostability under blue LED compared to **PNCs** and conventionally prepared $CsPbBr_3$ **CQDs** (**QD4**) (Fig. S5a–d†).

Screening and optimization of the photoredox reaction

To assess the photocatalytic utility of **QD1** in aromatization reactions under air, we selected Hantzsch ester *i.e.*, diethyl 2,6-dimethyl-1,4-dihydropyridine-3,5-dicarboxylate (**1a**) as a model substrate due to its synthetic accessibility. **1a** is also a popular NAD(P)H-type model for redox processes based on the dihydropyridine skeleton[43–45] and is well known in pharmacology as calcium channel blockers for curing cardiovascular diseases.[58,59] Furthermore, CV studies (Fig. S6†) show that the redox potential of **1a** is above the VBM of **QD1** and therefore, it acts as a potential hole accepting substrate for **QD1**.

To initiate the photocatalytic studies, **1a** was dissolved in dichloromethane (DCM) and illuminated with a blue LED lamp in the presence of a catalytic amount (1 mg) of **QD1**. NMR studies confirmed the formation of the aromatized product **2a** with 85% yield (Scheme 1). The reaction was carried out using off-the-shelf solvent, in air at room temperature without the
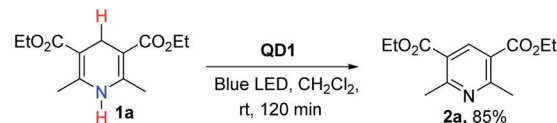
Scheme 1 Initial result of oxidative aromatization of **1a** in the presence of **QD1** acting as the photocatalyst.

use of an additional external oxidant. Although Hantzsch ester (**1a**) is a known hydrogen atom transfer (HAT) reagent, yet it is very slowly oxidized without the catalyst demonstrating the necessity to identify suitable catalysts.[45–47] In fact, the aromatization of **1a** performed in the absence of catalyst furnished **2a** in poor yield (20% yield, entry 3, Table S1†) implying the essential role of **QD1** to activate the organic substrate **1a**. We screened the reaction of **1a** under different synthetic conditions to optimize the catalytic efficiency of **QD1**. The results of the optimization studies are detailed in Table S1.† In the absence of light, only a trace amount of **2a** was detected confirming that the presence of light is necessary to favor the progress of reaction (entry 2, Table S1†). Different solvents of varying polarity and reactivity such as toluene, CHCl$_3$, 1,4-dioxan, THF, 1,2-dichloroethane (DCE) and ethyl acetate were also tested and the successful formation of **2a** from **1a** was observed in each case with high to excellent yields (entries 5–9, Table S1†). Although, the dispersion of **QD1** showed improved photostability in hexane as compared to DCE (Fig. S5†), the photocatalytic reaction was not performed in hexane solvent owing to its non-polar attributes. The precursors (organic substrates) were not soluble in hexane solvent. For the substrate **1a**, the best result in terms of reaction yield was observed in 1,2-dichloroethane (DCE) solvent affording the desired product **2a** in 95% yield. These parameters were marked as the optimum photocatalytic reaction conditions for further studies (entry 4, Table S1†).

Substrate scope: extension to the less reactive HAT reagents

The present photocatalytic protocol is highly efficient and compatible for aromatizing a broad range of heterocyclic substrates. In the following, we demonstrate the successful aromatization of a library of substrates consisting of substituted 1,4-DHP (**1a–j**), 1,2-DHP (**3a–f**), 2-aryl-2,3-dihydrobenzothiazole (**5a–c**) and 1,3,5-triaryl-pyrazoline (**7a–e**), using **QD1** under optimized reaction conditions (solvent: DCE, catalyst: 1 mg **QD1**, room temperature). Most significantly, the overwhelming majority of these substrates are poor HAT reagents compared to **1a** without the catalyst. In fact, only traces of product were detected even when reaction was prolonged to more than 5 h. With the catalyst, the reaction showed excellent yields at much shorter reaction times (86–95%, Fig. 2). Highly pure products were directly isolated from the reaction mixture *via* centrifugation, without the need of column chromatographic separation techniques. We observed that the reaction rates were different for different substituents, underlining the strong influence of the electronic nature of the substituents (R) on the progress (rate) of the reaction. To
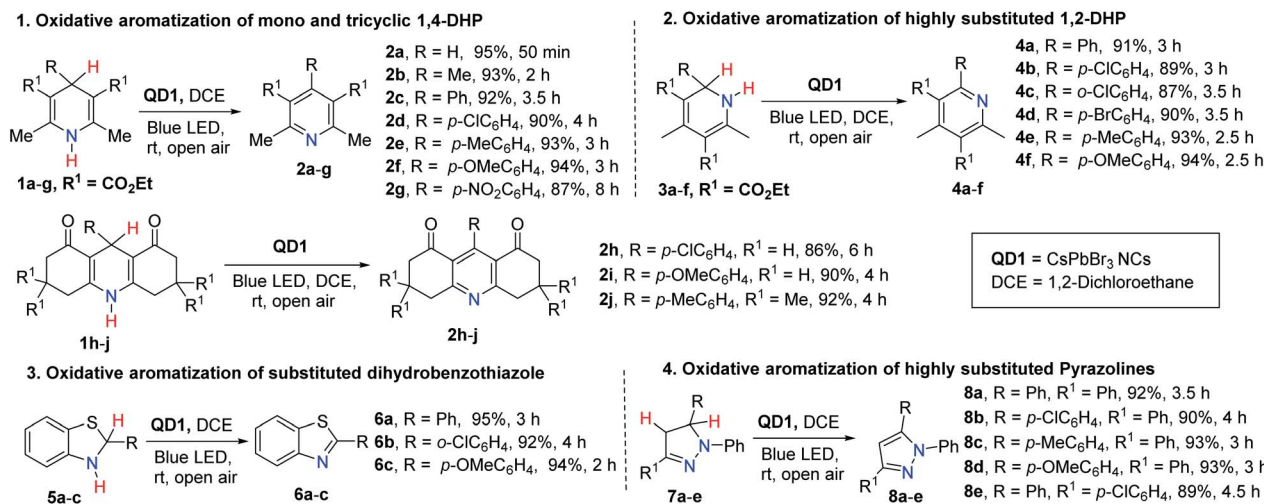
1. Oxidative aromatization of mono and tricyclic 1,4-DHP

2a, R = H, 95%, 50 min
2b, R = Me, 93%, 2 h
2c, R = Ph, 92%, 3.5 h
2d, R = p-ClC$_6$H$_4$, 90%, 4 h
2e, R = p-MeC$_6$H$_4$, 93%, 3 h
2f, R = p-OMeC$_6$H$_4$, 94%, 3 h
2g, R = p-NO$_2$C$_6$H$_4$, 87%, 8 h

2h, R = p-ClC$_6$H$_4$, R^1 = H, 86%, 6 h
2i, R = p-OMeC$_6$H$_4$, R^1 = H, 90%, 4 h
2j, R = p-MeC$_6$H$_4$, R^1 = Me, 92%, 4 h

2. Oxidative aromatization of highly substituted 1,2-DHP

4a, R = Ph, 91%, 3 h
4b, R = p-ClC$_6$H$_4$, 89%, 3 h
4c, R = o-ClC$_6$H$_4$, 87%, 3.5 h
4d, R = p-BrC$_6$H$_4$, 90%, 3.5 h
4e, R = p-MeC$_6$H$_4$, 93%, 2.5 h
4f, R = p-OMeC$_6$H$_4$, 94%, 2.5 h

QD1 = CsPbBr$_3$ NCs
DCE = 1,2-Dichloroethane

3. Oxidative aromatization of substituted dihydrobenzothiazole

6a, R = Ph, 95%, 3 h
6b, R = o-ClC$_6$H$_4$, 92%, 4 h
6c, R = p-OMeC$_6$H$_4$, 94%, 2 h

4. Oxidative aromatization of highly substituted Pyrazolines

8a, R = Ph, R^1 = Ph, 92%, 3.5 h
8b, R = p-ClC$_6$H$_4$, R^1 = Ph, 90%, 4 h
8c, R = p-MeC$_6$H$_4$, R^1 = Ph, 93%, 3 h
8d, R = p-OMeC$_6$H$_4$, R^1 = Ph, 93%, 3 h
8e, R = Ph, R^1 = p-ClC$_6$H$_4$, 89%, 4.5 h

Fig. 2 Aromatization of a broad variety of substrates comprising 1,4-DHP, 1,2-DHP, dihydrobenzothiazole and pyrazoline derivatives catalyzed by QD1 photocatalyst under blue light irradiation affording a library of corresponding aromatized azaheterocycles. The maximum absorption wavelength and the illumination intensity of the blue LED light (40 W) are 461 nm and 0.363 mW cm^{-2} at a distance of 100 cm respectively.

understand the quantitative relation between structure and reactivity, detailed kinetic studies were performed on 1,4-DHP based substrates.

Structure-reactivity correlation study

We observed that the rate of oxidative aromatization was faster in the presence of electron donating groups (EDGs) and the reverse effect was noted in the presence of electron withdrawing groups (EWGs) as the substituent. Evidently, kinetic studies reveal that the reaction rate constants of *para*-substituted 1,4-aryl-DHP (**1c–1g**) (R = p-X-C$_6$H$_4$, where X = OMe, Me, H, Cl and
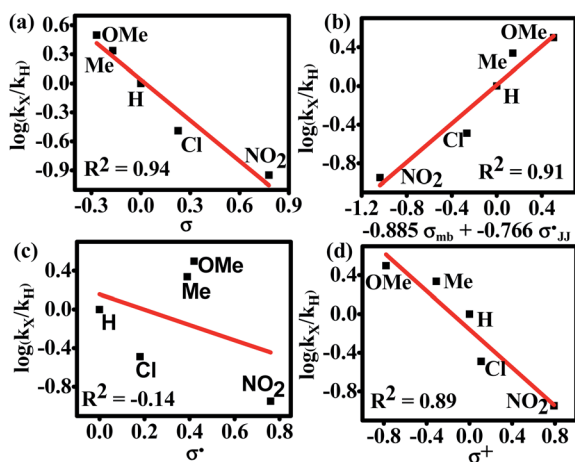

Fig. 3 Hammett single and dual correlations of the aromatization of *para*-substituted 1,4-aryl-DHP such as **1c** (H), **1d** (Cl), **1e** (Me), **1f** (OMe), and **1g** (NO$_2$). (a) Simple Hammett plot corroborating the influence of the inductive effect of the substituents on reactivity; (b) construction of the Hammett plot employing Jiang's dual-parameter; (c) non-linear correlation of the Hammett plot of log(K_X/K_H) versus $\sigma^{\bullet}$ indicating no spin delocalization; (d) Hammett plot of log(K_X/K_H) versus σ^+ signifying the dominance of polar effects over spin delocalization effects.

NO$_2$) decreases four fold as the *para*-substituent becomes progressively more electron withdrawing (Fig. S7 and Tables S2, S3†). Applying the Hammett equation for this transformation, a linear relationship between logarithms of first order rate constant and Hammett substituent constant (σ)[60] was observed, corroborating the strong electronic effect (Fig. 3a). To obtain deeper mechanistic insights from these kinetic data, the more advanced Jiang's dual-parameter[61] that considers both polar and spin delocalization effects was used (Fig. 3b). Again, a linear correlation was obtained using a Jiang's dual-parameter, underlining the possible involvement of both ionic and/or radical intermediates in the reaction. In Jiang's dual-parameter formalism, positive ln(k_X/k_H) experimental values suggest that the reaction is accelerated by EWGs and *vice versa*. The negative value of the polar reaction constant ($\rho_{mb} = -0.885$) indicates a modest positive charge developed in the transition state, while the negative spin delocalization constant ($\rho_{JJ}^{\bullet} = -0.766$) suggests that *para*-substitution has no effect on the delocalization of the radical formed during the reaction. The ratio of the constants ($\rho_{mb}/\rho_{JJ}^{\bullet}$) which is slightly more than unity (1.15) strongly indicates that the polar delocalization effect is more dominant compared to the spin delocalization effect. This observation is further corroborated by the fact that a non-linear correlation (Fig. 3c) was obtained when only spin delocalization parameters were considered, whereas a linear correlation was obtained when only polar substitution was considered (Fig. 3d). In other words, these data suggest that the reaction possibly proceeds *via* radical cation or radical anion intermediates where the electronic effect on reactivity is predominant due to polar effects.

Driving force and mechanism

CV studies on four different model azaheterocycle substrates suggested that most of these heterocycles are potential hole acceptors with their redox potential value well above the VBM of
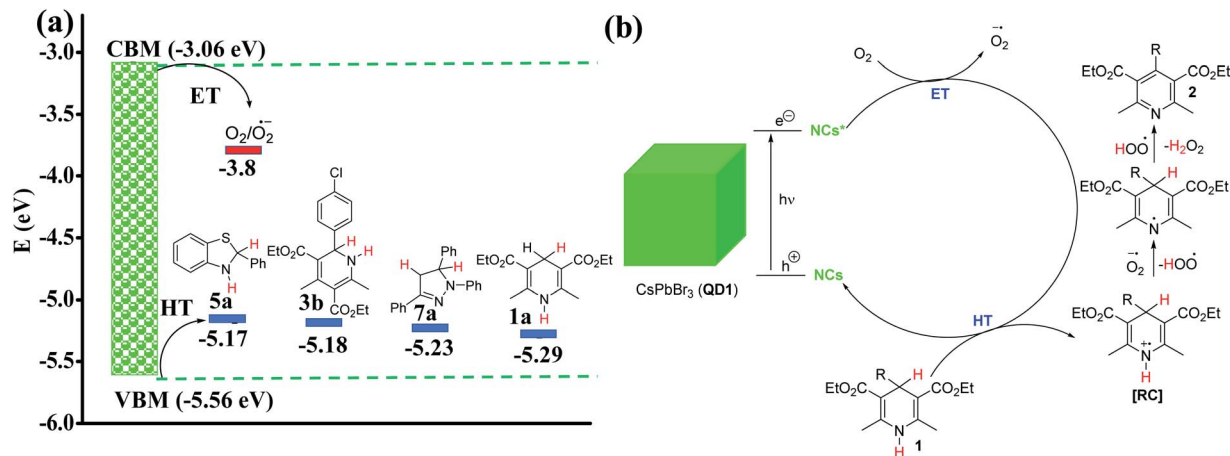
Fig. 4 (a) Redox potential (eV) of different substrates compared to the valence band maximum (VBM) and conduction band minimum (CBM) of QD1. The data obtained from cyclic voltammetry is marked with blue bars and the literature value for the $O_2/O_2^{\bullet-}$ redox pair by a red bar. The measured potentials (V) from CV were converted to HOMO/LUMO energy levels (eV) with respect to a Fc/Fc$^+$ reference (-4.8 eV to vacuum);[62,63] (b) plausible mechanism for the formation of aromatized products (2) in the presence of QD1 as photocatalyst under blue light irradiation. (RC = radical cation, ET = electron transfer and HT = hole transfer).

the QD1 (Fig. S6, S11b, S12 and S15†). The driving force for electron and hole transfer is provided in Fig. 4a based on electrochemical data. The hole accepting tendency of the substrate is further confirmed by Stern–Volmer studies[64] (Fig. S21†). Since the reaction takes place in the presence of air and based on the redox potential values it is safe to conclude that oxygen accepts the electron from the excited QD1 photocatalyst to form a superoxide anion radical $[O_2^{\bullet-}]$ intermediate,[33–35] while the substrate (1) accepts the hole to form a radical cation intermediate (RC). This leads to the successful charge separation and activation of the substrate. The *in situ* generated superoxide anion radical is responsible for the subsequent aromatization of RC to deliver the corresponding aromatized product (2) along with the production of H_2O_2 (Fig. 4b). A similar mechanism operates for the aromatization of the other substrates such as 3, 5 and 7 (Fig. S22a and b†). The proposed mechanism is also consistent with the previous reports.[35,48] Additionally, QD1 catalysed photo-aromatization of 1c (a control experiment) was performed under nitrogen atmosphere, using solvents purged with the nitrogen gas. As expected, the formation of the product 2c was suppressed considerably under strictly air-free conditions. However, the same reaction under open air condition afforded the aromatized product 2c in 92% yield in 3.5 h (Fig. S23†) indicating the key role of O_2 in aromatizing the organic substrate. Direct evidence of the radical intermediate was achieved using 2,2,6,6-tetramethyl-1-piperidinyloxy (TEMPO), which is a widely used radical scavenger. In the presence of TEMPO, the photo-aromatization of 1a was significantly suppressed yielding only 30% of product within 2 h compared to 95% in 50 min in the absence of the radical quencher. The proposed mechanism is further supported by the detection of H_2O_2 in the reaction mixture (Fig. S24†). It is well-known that 3,3′,5,5′-tetramethylbenzidine (TMB) gives a blue colored diimine complex with a maximum absorbance at 652 nm in the presence of H_2O_2.[65,66]

To confirm the formation of H_2O_2 in our reaction, we mixed TMB with the extract of the reaction solution after 1 h of the aromatization reaction of 1a in acetate buffer (pH = 4) and monitored the UV-Vis absorbance during 12 h. The detection and evolution of the characteristic peak at 652 nm confirms the formation of H_2O_2. We also performed control experiments with laboratory grade 30% H_2O_2 and without H_2O_2 under similar conditions to rule out any ambiguity.

Comparison of the catalytic activity of QD1 with other photocatalysts

For comparison, oxidative aromatization of 1b was carried out in the presence of various commonly used state-of-the-art catalysts such as the ruthenium complex ([Ru(bpy)$_3$][PF$_6$]$_2$),[67] polydisperse CsPbBr$_3$ NCs (PNCs)[14,18] and rhodamine 6G (Rh-6G).[68,69] The photocatalysts were either purchased or synthesized using standard literature protocols and thoroughly characterized using UV-Vis spectroscopy, PL, NMR or TEM wherever it was applicable (Fig. S25–S28†). The kinetic data were obtained by monitoring the progress of the oxidative aromatization of 1b using UV-Vis absorption spectroscopy (Fig. S29†). The gradual decrease of the distinct absorption peak at 339 nm as a function of time signifies of the substrate and progress of the reaction. Fig. 5a compares the reaction rate of QD1 with those of other photocatalysts. The pseudo first order rate constants (k) were calculated by plotting $\ln(C_t/C_0)$ as a function of the reaction time. Polydisperse CsPbBr$_3$ NCs (PNCs) are air-stable with higher catalytic efficiency, compared to conventionally prepared LHP QDs, transition metal complexes and other state-of-the-art quantum dots.[14,18] In their detailed work, Yan and co-workers have demonstrated the use of PNCs for a wide range of organic transformations including C–C, C–N and C–O bond formations.[14,18] In our case, as expected, compared to the conventionally prepared QD4 and the Ru-based molecular complex [Ru(bpy)$_3$][PF$_6$]$_2$, the (2–5 times) higher rate of reaction

was noted when **PNCs** were applied as the catalyst under similar conditions. The lower reaction rate in the presence of **QD4** is attributed to its poor stability. The XRD studies revealed that **QD4** underwent a complete degradation within 10 days under ambient condition to a mixture of tetragonal $CsPb_2Br_5$ and orthorhombic $CsPbBr_3$ phases (Fig. S26†). Interestingly, halide-passivated **QD1** shows an even higher (two-fold) rate compared to **PNCs**. We underline that these results were highly reproducible and consistent using different batches of catalyst samples prepared under the same conditions. The observed rate increase is attributed to ultrafast interfacial electron and hole transfer,[6] the increase of the surface area and the more homogeneous nature of **QD1** as compared to **PNCs**. The difference in efficiency was even more dramatic in substrates with EWG (**1g**). To give an example, the oxidative aromatization of **1g** with R = p-NO_2–C_6H_4 at 4 position as EWG using **PNCs** was unsuccessful even after 8 h. On the other hand, the same reaction resulted in 85% yield with **QD1** under the same conditions. This stark difference can be attributed to the more favorable band alignment of **QD1** with respect to the redox potential of substrate **1g**, favoring the hole transfer (Fig. 5b). Due to quantum confinement effects, **QD1** has a slightly higher band gap compared to **PNCs** as demonstrated in Fig. 5b. Furthermore, **QD1** was 5 times more efficient as compared to the Ru-based transition metal complexes (Fig. 5a). $[Ru(bpy)_3][PF_6]_2$ is widely used as photocatalyst in various organic transformations and is also a known photocatalyst for the oxidative aromatization reaction. Therefore, the direct comparison of **QD1** with $[Ru(bpy)_3][PF_6]_2$ gives us insight into the catalytic potential of **QD1** for organic transformations in general. We attribute the better catalytic efficiency of **QD1** over these molecular catalysts to its strong O_2-tolerance. The efficiency of $Ru(bpy)_3^{2+}$ is known to diminish in O_2-rich conditions due to the strong competition between the quenching of the catalyst by O_2 and the catalytic reaction, thereby demanding N_2-sparging.[70] We also employed Rh-6G, a popular air-tolerant organic dye,[68,69] for comparison. Compared to Rh-6G we found 3 times higher reaction rate with **QD1**, indicating that these LHP based QDs have a high potential

as alternatives to existing molecular catalysts for use in various organic transformations.

Consistent with the kinetic data above, **QD1** demonstrated a higher turnover number (TON) compared to **PNCs** and conventionally synthesized **QD4**. 0.1 mmol of **1a** and **QD1** (1 mg) in 3 mL of DCE were subjected to blue light irradiation (procedure detailed in Fig. S30 and S31†) for 4 consecutive cycles and the yield of the aromatized product (**2a**) was determined for each cycle using ^{1}H NMR analysis of the crude reaction mixture. The reaction yielded 96%, 93%, 86% and 70% for 1st, 2nd, 3rd and 4th cycle, respectively, indicating that the catalytic activity of **QD1** remained robust at least for 4 cycles. However, **QD1** on long exposure to the polar solvent (DCE) and light under optimal reaction condition undergoes degradation due to the desorption of the passivating agents (bromide, oleic acid and oleylamine) from the surface of **QD1** minimizing its stability. The presence of capping ligands on the surface of the QDs plays a decisive role in imparting the long-term stability of QDs.[71] The TON of **QD1** (200) was higher than that of the polydisperse NCs (**PNCs**, TON = 177) and of conventionally synthesized $CsPbBr_3$ NCs (**QD4**, TON = 166) for the aromatization of **1a** under optimized reaction conditions (Table 1). The TON was calculated based on molecular weight of $CsPbBr_3$ (579.8 g mol^{-1}, for details see ESI note†).[18] Finally, we studied the comparative efficiency of the three different sized **CQDs** (**QD1**, **QD2** and **QD3**) (Fig. S32†) using **1b**. As expected, compared to **QD1**, larger sized **CQDs** (**QD2**) showed a slower

Table 1 Comparison of the TON of **QD1** with polydisperse $CsPbBr_3$ NCs (**PNCs**) and with conventionally prepared $CsPbBr_3$ **CQDs** (**QD4**) for the aromatization of **1a**

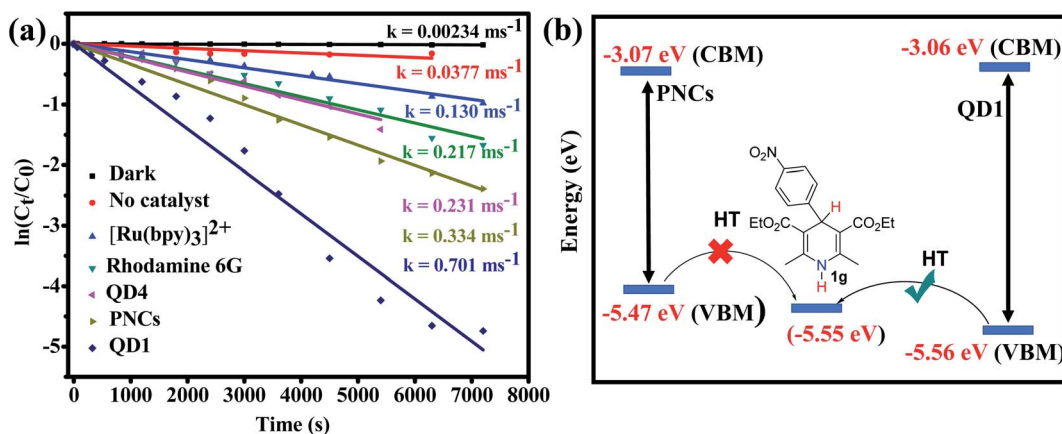| Photo-catalyst	Yield% (1st cycle)	Yield% (2nd cycle)	Yield% (3rd cycle)	Yield% (4th cycle)	TON
QD1	96	93	86	70	200
PNCs	91	79	74	62	177
QD4	93	72	69	53	166

Fig. 5 (a) Plots of $\ln(C_t/C_0)$ versus reaction time of the aromatization of **1b** comparing the catalytic activity of **QD1** with other photocatalysts; (b) more advantageous band alignment of **QD1** with respect to bulk-type **PNCs** favouring hole transfer to substrates containing strong EWGs (**1g**). CBM and VBM for **QD1** obtained from cyclic voltammetry and for **PNCs** from the literature.[18]

reaction rate, which is ascribed to the decrease of the surface area in the latter and/or to the less favorable energy level alignment due to reduced quantum confinement.[18] With smaller **CQDs** (**QD3**) the observed decrease of the catalytic efficiency appears at a first glance surprising. It is likely due to the decrease of the air-stability with decreasing size.[18] We noticed that smaller **CQDs** (**QD3**) have poor photostability compared to larger ones (**QD1**), possibly due to the lower temperature synthetic conditions employed. In fact, previous studies have demonstrated that pronounced stability of LHP **CQDs** was only observed at high temperature synthetic conditions.[22]

Conclusions

Despite the recent surge of development in synthetic protocols, mainly aimed at improving performances in optoelectronic devices, to date the wide application of LHP **CQDs** as photocatalysts in organic synthesis is not successful, mainly due to their poor air- and photostability. Here we demonstrated that stable LHP **CQDs** prepared under optimum temperature and halide-rich conditions are very promising photocatalysts for organic transformation. We tested the applicability of these **CQDs** by carrying out oxidative aromatization of a variety of azaheterocycles in air using off-the-shelf substrates and solvent. They outperform many state-of-the-art molecular and nanomaterials-based catalysts in terms of reaction rate, yield, reusability and turnover number. The variation of the substituents of the substrates showed that the rate of oxidative aromatization was faster in the presence of electron donating groups. Further analysis of the kinetic data indicated the presence of radical cation or radical anion intermediates and the predominance of electronic effects governing the reactivity. Our study also unraveled the underlying mechanisms confirming the role of the azaheterocycle substrates as hole acceptors and that of ambient oxygen as electron acceptor from photoexcited LHP **CQDs** culminating in the aromatization of the substrate and concomitant liberation of H_2O_2. Both high photo- and chemical stability as well as favorable energy level alignment of the QDs with respect to the organic substrate are required to achieve efficient photocatalysis. Concluding, this study provides a significant step towards the practical applicability of energy-level tunable, size-controlled LHP **CQDs** as efficient photocatalysts in organic synthesis. We expect that these stable **CQDs** are equally effective for C–C, C–O, C–N, C–S bond formation, C–H functionalization, thiol coupling and various other important organic reactions.

Conflicts of interest

There are no conflicts to declare.

Acknowledgements

References

1 H. Huang, M. I. Bodnarchuk, S. V. Kershaw, M. V. Kovalenko and A. L. Rogach, *ACS Energy Lett.*, 2017, **2**, 2071–2083.

2 Y. Wang, X. Li, J. Song, L. Xiao, H. Zeng and H. Sun, *Adv. Mater.*, 2015, **27**, 7101–7108.

3 J. S. Manser, J. A. Christians and P. V. Kamat, *Chem. Rev.*, 2016, **116**, 12956–13008.

4 Q. A. Akkerman, G. Rainò, M. V. Kovalenko and L. Manna, *Nat. Mater.*, 2018, **17**, 394–405.

5 X. Zhang, H. Lin, H. Huang, C. Reckmeier, Y. Zhang, W. C. H. Choy and A. L. Rogach, *Nano Lett.*, 2016, **16**, 1415–1420.

6 K. Wu, G. Liang, Q. Shang, Y. Ren, D. Kong and T. Lian, *J. Am. Chem. Soc.*, 2015, **137**, 12792–12795.

7 Y. Wu, X. Yang, W. Chen, Y. Yue, M. Cai, F. Xie, E. Bi, A. Islam and L. Han, *Nat. Energy*, 2016, **1**, 16148.

8 J. B. Hoffman, G. Zaiats, I. Wappes and P. V. Kamat, *Chem. Mater.*, 2017, **29**, 9767–9774.

9 A. Swarnkar, A. R. Marshall, E. M. Sanehira, B. D. Chernomordik, D. T. Moore, J. A. Christians, T. Chakrabarti and J. M. Luther, *Science*, 2016, **354**, 92–95.

10 T. C. Sum and N. Mathews, *Energy Environ. Sci.*, 2014, **7**, 2518–2534.

11 J. Burschka, N. Pellet, S. J. Moon, R. Humphry-Baker, P. Gao, M. K. Nazeeruddin and M. Grätzel, *Nature*, 2013, **499**, 316–319.

12 Q. Tai, K. C. Tang and F. Yan, *Energy Environ. Sci.*, 2019, **12**, 2375–2405.

13 Y. Cheng, F. So and S. W. Tsang, *Mater. Horiz.*, 2019, **6**, 1611–1624.

14 X. Zhu, Y. Lin, Y. Sun, M. C. Beard and Y. Yan, *J. Am. Chem. Soc.*, 2019, **141**, 733–738.

15 K. Chen, X. Deng, G. Dodekatos and H. Tüysüz, *J. Am. Chem. Soc.*, 2017, **139**, 12267–12273.

16 H. Lu, X. Zhu, C. Miller, J. San Martin, X. Chen, E. M. Miller, Y. Yan and M. C. Beard, *J. Chem. Phys.*, 2019, **151**, 204305.

17 Y. F. Xu, M. Z. Yang, B. X. Chen, X. D. Wang, H. Y. Chen, D. Bin Kuang and C. Y. Su, *J. Am. Chem. Soc.*, 2017, **139**, 5660–5663.

18 X. Zhu, Y. Lin, J. San Martin, Y. Sun, D. Zhu and Y. Yan, *Nat. Commun.*, 2019, **10**, 2843.

19 W.-B. Wu, Y.-C. Wong, Z.-K. Tan and J. Wu, *Catal. Sci. Technol.*, 2018, **8**, 4257–4263.

20 L. Protesescu, S. Yakunin, M. I. Bodnarchuk, F. Krieg, R. Caputo, C. H. Hendon, R. X. Yang, A. Walsh and M. V Kovalenko, *Nano Lett.*, 2015, **15**, 3692–3696.

21 A. Dutta, S. K. Dutta, S. Das Adhikari and N. Pradhan, *ACS Energy Lett.*, 2018, **3**, 329–334.

22 S. Thapa, K. Bhardwaj, S. Basel, S. Pradhan, C. J. Eling, A. M. Adawi, J.-S. G. Bouillard, G. J. Stasiuk, P. Reiss, A. Pariyar and S. Tamang, *Nanoscale Adv.*, 2019, **1**, 3388–3391.

23 K. Zhou and Y. Li, *Angew. Chem., Int. Ed.*, 2012, **51**, 602–613.

24 R. Long, K. Mao, X. Ye, W. Yan, Y. Huang, J. Wang, Y. Fu, X. Wang, X. Wu, Y. Xie and Y. Xiong, *J. Am. Chem. Soc.*, 2013, **135**, 3200–3207.

25 Z. Quan, Y. Wang and J. Fang, *Acc. Chem. Res.*, 2013, **46**, 191–202.

26 J. Y. Woo, Y. Kim, J. Bae, T. G. Kim, J. W. Kim, D. C. Lee and S. Jeong, *Chem. Mater.*, 2017, **29**, 7088–7092.

27 C. Wang, A. S. R. Chesman and J. J. Jasieniak, *Chem. Commun.*, 2017, **53**, 232–235.

28 A. Dutta, S. K. Dutta, S. Das Adhikari and N. Pradhan, *Angew. Chem., Int. Ed.*, 2018, **57**, 9083–9087.

29 J. Pan, Y. Shang, J. Yin, M. De Bastiani, W. Peng, I. Dursun, L. Sinatra, A. M. El-zohry, M. N. Hedhili, A. Emwas, O. F. Mohammed, Z. Ning and O. M. Bakr, *J. Am. Chem. Soc.*, 2018, **140**, 562–565.

30 H. Sun, Z. Li, L. Kong, B. Wang, C. Zhang, Q. Yuan, S. Huang, Y. Liu and L. Li, *Chem. Commun.*, 2018, **54**, 9345–9348.

31 B. Li, Y. Zhang, L. Fu, T. Yu, S. Zhou, L. Zhang and L. Yin, *Nat. Commun.*, 2018, **9**, 1076.

32 A. Dutta and N. Pradhan, *ACS Energy Lett.*, 2019, **4**, 709–719.

33 M. Hayyan, M. A. Hashim and I. M. Alnashef, *Chem. Rev.*, 2016, **116**, 3029–3085.

34 A. S. Jalilov, C. Zhang, E. L. G. Samuel, W. K. A. Sikkema, G. Wu, V. Berka, T. A. Kent, A. L. Tsai and J. M. Tour, *ACS Appl. Mater. Interfaces*, 2016, **8**, 15086–15092.

35 K. Gu, Y. Wang, J. Shen, J. Zhu, Y. Zhu and C. Li, *ChemSusChem*, 2020, **13**, 682–687.

36 F. Lang, O. Shargaieva, V. V. Brus, H. C. Neitzert, J. Rappich and N. H. Nickel, *Adv. Mater.*, 2018, **30**, 1702905.

37 C. C. Boyd, R. Cheacharoen, T. Leijtens and M. D. McGehee, *Chem. Rev.*, 2019, **119**, 3418–3451.

38 S. Aiello, G. Wells, E. L. Stone, H. Kadri, R. Bazzi, D. R. Bell, M. F. G. Stevens, C. S. Matthews, T. D. Bradshaw and A. D. Westwell, *J. Med. Chem.*, 2008, **51**, 5135–5139.

39 C. Allais, J. M. Grassot, J. Rodriguez and T. Constantieux, *Chem. Rev.*, 2014, **114**, 10829–10868.

40 Y. Yan, J. Yang, Z. Yu, M. Yu, Y. T. Ma, L. Wang, C. Su, J. Luo, G. P. Horsman and S. X. Huang, *Nat. Commun.*, 2016, **7**, 13083.

41 L. Da Costa, E. Scheers, A. Coluccia, M. Casulli, M. Roche, C. Di Giorgio, J. Neyts, T. Terme, R. Cirilli, G. La Regina, R. Silvestri, C. Mirabelli and P. Vanelle, *J. Med. Chem.*, 2018, **61**, 8402–8416.

42 T. Wu, C. Jiang, L. Wang, S. L. Morris-Natschke, H. Miao, L. Gu, J. Xu, K. H. Lee and Q. Gu, *J. Nat. Prod.*, 2015, **78**, 1593–1599.

43 F. P. Guengerich, M. V. Martin, P. H. Beaune, P. Kremers, T. Wolff and D. J. Waxman, *J. Biol. Chem.*, 1986, **261**, 5051–5060.

44 D. M. Stout and A. I. Meyers, *Chem. Rev.*, 1982, **82**, 223–243.

45 X. Q. Zhu, B. J. Zhao and J. P. Cheng, *J. Org. Chem.*, 2000, **65**, 8158–8163.

46 N. Nakamichi, Y. Kawashita and M. Hayashi, *Org. Lett.*, 2002, **4**, 3955–3957.

47 D. Zhang, L. Z. Wu, L. Zhou, X. Han, Q. Z. Yang, L. P. Zhang and C. H. Tung, *J. Am. Chem. Soc.*, 2004, **126**, 3440–3441.

48 R. Ananthakrishnan and S. Gazi, *Catal. Sci. Technol.*, 2012, **2**, 1463–1471.

49 M. Imran, V. Caligiuri, M. Wang, L. Goldoni, M. Prato, R. Krahne, L. De Trizio and L. Manna, *J. Am. Chem. Soc.*, 2018, **140**, 2656–2664.

50 Q. A. Akkerman, L. Mart, L. Goldoni, M. Imran, D. Baranov, H. J. Bolink, F. Palazon and L. Manna, *Chem. Mater.*, 2018, **30**, 6915–6921.

51 J. Butkus, P. Vashishtha, K. Chen, J. K. Gallaher, S. K. K. Prasad, D. Z. Metin, G. Laufersky, N. Gaston, J. E. Halpert and J. M. Hodgkiss, *Chem. Mater.*, 2017, **29**, 3644–3652.

52 B. Zorman, M. V. Ramakrishna and R. A. Friesner, *J. Phys. Chem.*, 1995, **99**, 7649–7653.

53 X. Luo, R. Lai, Y. Li, Y. Han, G. Liang, X. Liu, T. Ding, J. Wang and K. Wu, *J. Am. Chem. Soc.*, 2019, **141**, 4186–4190.

54 Y. Dong, T. Qiao, D. Kim, D. Parobek, D. Rossi and D. H. Son, *Nano Lett.*, 2018, **18**, 3716–3722.

55 V. K. Ravi, G. B. Markad and A. Nag, *ACS Energy Lett.*, 2016, **1**, 665–671.

56 D. Yoo, J. Y. Woo, Y. Kim, S. W. Kim, S. H. Wei, S. Jeong and Y. H. Kim, *J. Phys. Chem. Lett.*, 2020, **11**, 652–658.

57 J. Liu, K. Song, Y. Shin, X. Liu, J. Chen, K. X. Yao, J. Pan, C. Yang, J. Yin, L. J. Xu, H. Yang, A. M. El-Zohry, B. Xin, S. Mitra, M. N. Hedhili, I. S. Roqan, O. F. Mohammed, Y. Han and O. M. Bakr, *Chem. Mater.*, 2019, **31**, 6642–6649.

58 D. Vo, W. C. Matowe, M. Ramesh, N. Iqbal, M. W. Wolowyk, S. E. Howlett and E. E. Knaus, *J. Med. Chem.*, 1995, **38**, 2851–2859.

59 R. H. Bocker and F. P. Guengerich, *J. Med. Chem.*, 1986, **29**, 1596–1603.

60 D. H. McDaniel and H. C. Brown, *J. Org. Chem.*, 1958, **23**, 420–427.

61 X. K. Jiang, *Acc. Chem. Res.*, 1997, **30**, 283–289.

62 C. Fujisue, T. Kadoya, T. Higashino, R. Sato, T. Kawamoto and T. Mori, *RSC Adv.*, 2016, **6**, 53345–53350.

63 M. L. Tang, A. D. Reichardt, P. Wei and Z. Bao, *J. Am. Chem. Soc.*, 2009, **131**, 5264–5273.

64 F. C. L. Luiz, L. S. Garcia, L. S. G. Filho, L. R. Teixeira and S. R. W. Louro, *J. Fluoresc.*, 2011, **21**, 1933–1940.

65 L. Gao, J. Wu and D. Gao, *ACS Nano*, 2011, **5**, 6736–6742.

66 D. Josephy, T. Eling and R. Mason, *J. Biol. Chem.*, 1982, **257**, 3669–3675.

67 C. K. Prier, D. A. Rankic and D. W. C. MacMillan, *Chem. Rev.*, 2013, **113**, 5322–5363.

68 I. Ghosh and B. König, *Angew. Chem., Int. Ed.*, 2016, **55**, 7676–7679.

69 M. Beija, C. A. M. Afonso and J. M. G. Martinho, *Chem. Soc. Rev.*, 2009, **38**, 2410–2433.

70 M. A. Cismesia and T. P. Yoon, *Chem. Sci.*, 2015, **6**, 5426–5434.

71 R. Grisorio, M. E. Di Clemente, E. Fanizza, I. Allegretta, D. Altamura, M. Striccoli, R. Terzano, C. Giannini, M. Irimia-Vladu and G. P. Suranna, *Nanoscale*, 2019, **11**, 986–999.